JOURNAL OF GEOPHYSICAL RESEARCH, VOL. 100, NO. A12, PAGES 23,543–23,549, DECEMBER 1, 1995

Electron trajectories in a model magnetosphere: Simulation and observation under active conditions

Zhongmin Lin, John W. Bieber, and Paul Evenson
Bartol Research Institute, University of Delaware, Newark

Abstract. Trajectories of electrons with energies of 10–2000 MeV were studied using Tsyganenko's global quantitative model of the magnetosphere. Results were compared with balloon observations of atmospheric, return albedo, and cosmic electrons made at Prince Albert on August 26, 1987. Active geomagnetic conditions were associated with unusual variations in the flux of electrons on that date, which we interpret as a manifestation of an anomalously low and highly variable geomagnetic cutoff. Increasing the ring current intensity in the Tsyganenko model reduces the calculated effective cutoff rigidity somewhat, but to explain all of our observations, we must postulate that trajectories traditionally assumed to be forbidden are sometimes systematically converted into allowed trajectories. Within this model we can also identify field lines on which bursts of auroral X rays were generated.

Introduction

Balloon-borne instruments have been used to study cosmic and atmospheric secondary radiation for many years [*Pfotzer*, 1936a, b; *Jokipii et al.*, 1967; *Verma*, 1967; *Israel et al.*, 1968; *Israel*, 1969; *Hovestadt and Meyer*, 1970; *Berger and Seltzer*, 1972; *Fulks and Meyer*, 1974; *Daniel and Stephens*, 1974; *Matthews et al.*, 1988]. The electron flux shows a broad maximum at around 100 g/cm^2 atmospheric depth. *Pfotzer* [1936a, b] interpreted this phenomenon as a superposition of an attenuated cosmic component and the buildup and subsequent attenuation of secondary particles produced in the atmosphere. The main sources of secondary electrons in the atmosphere are decay of short-lived particles, including radioactive nuclei, created during collisions of cosmic rays with air nuclei and ejection of "knock-on" electrons by cosmic ray nuclei, pions, and muons [*Daniel and Stephens*, 1974].

Some secondary electrons produced in the atmosphere move upward and are usually referred to as "splash albedo" electrons. Like cosmic electrons, their propagation is strongly influenced by the geomagnetic field. Splash albedo electrons that have rigidities higher than the local geomagnetic cutoff escape from the magnetosphere, but those with rigidities below this cutoff eventually reenter the atmosphere and are then referred to as "return albedo" electrons. This results in the observed diurnal intensity variations of low-energy electrons, in which high fluxes are observed during the day and low fluxes at night. *Jokipii et al.* [1967] attributed this to changes in the magnetosphere with local time, concluding that the high electron flux observed during the day consisted mainly of return albedo electrons which were absent at night.

In this paper, we present simulations of electron and positron trajectories using the appropriate International or Definitive Geomagnetic Reference Field (IGRF or DGRF) model [*Langel*, 1991] of the internal field, and the *Tsyganenko* [1987] model magnetospheric field to explore the dependence of three different trajectory classes upon geomagnetic activity.

Copyright 1995 by the American Geophysical Union.

Paper number 95JA02696.
0148-0227/95/95JA-02696$05.00

We use these calculations to interpret electron and X ray observations obtained during a high altitude balloon flight from Prince Albert (53.22° geographic latitude, and 254.07° geographic longitude) on August 26 and 27, 1987. Our calculations confirm the observation of lowered geomagnetic cutoffs when geomagnetic conditions are disturbed ($Kp \geq 4-$). However, even with some ad hoc adjustment, the Tsyganenko model does not seem to reproduce quantitatively the measured cutoffs. We look in detail at an episode of activity beginning at about 1050 UT on August 26, 1987, and conclude that the discrepancy lies in a band of computationally undetermined trajectories that change character systematically in response to some as yet undetermined magnetospheric structure or process. The transition from one state to the other was associated with a strong burst of auroral X rays, most probably originating on a field line at $L = 5$, that occurred about 1200 UT on August 26.

Trajectory Tracing Algorithm

Trajectory simulations in a model geomagnetic field are useful in order to study the access of particles into the different regions of the magnetosphere, for deriving cutoff rigidity at selected locations, and for determining particle sources [*McCracken et al.*, 1962; *Sauer*, 1963; *Shea and Smart*, 1967, 1975, 1990; *Gall et al.*, 1968, 1982; *Smart et al.*, 1969a, b; *Flindt*, 1970; *Imhof et al.*, 1971; *Flückiger et al.*, 1991; *Guzik et al.*, 1991; *Cooke et al.*, 1991; *Bieber et al.*, 1992; *Lin et al.*, 1993]. *McCracken et al.* [1962] first calculated particle trajectories in complex simulations of the geomagnetic field. *Shea et al.* [1965] studied vertical cutoff rigidities at more than 300 locations using sixth degree simulations of the geomagnetic field and defined the effective cutoff rigidity P_c. *Smart et al.* [1969a] combined an external field described by *Williams and Mead* [1965] with a sixth degree simulation of the internal geomagnetic field in order to calculate cutoff rigidities in the polar regions.

The common starting point of all of these calculations is the knowledge that if the charge sign and velocity of a particle are simultaneously reversed, the propagation equations remain unchanged. Thus one can determine trajectories of incident

particles by calculating trajectories of oppositely charged particles with the same rigidity shooting from the Earth. This now typical method for trajectory tracing was developed by *McCracken et al.* [1962], who used the Runge-Kutta method of integration.

In this paper, we use a modified technique to trace charged particles in the magnetic field. We assume that motion of a particle within a sufficiently small region is accurately approximated by the helical motion of the same particle in a uniform magnetic field. To obtain satisfactory accuracy, very small integration steps must be chosen. In our trajectory tracing code, the integration step size is varied adaptively along the trajectory as is done in most modern codes.

Effects of electric fields are neglected. For instance, if the total potential drop across the magnetosphere is 200 kV, then the average electric field is ~1 mV/m at 10 R_E. If the magnetic field at the same location is ~20 nT, then the ratio of electric to magnetic forces acting on a relativistic particle is $\sim 2 \times 10^{-4}$. As discussed later, however, electric forces even at this level may be a potentially important perturbing force for borderline trajectories.

The overall numerical strategy is as follows: Given a particle with position vector $\mathbf{x}$ and velocity vector $\mathbf{V}$ at step n, we first make a guess at the midpoint between steps n and $n + 1$ (which we call step $n + 1/2$) using a straight-line projection of the velocity vector. The magnetic field at the midpoint is then compared with the last magnetic field point (step $n - 1/2$) to obtain the field gradient. The new time step size is then adaptively chosen to make the field variation along the particle trajectory a small fraction of the total field. Conceptually, we choose the time step Δt to satisfy

$$|(\mathbf{V}\Delta t) \cdot \nabla \mathbf{B}| = \varepsilon |\mathbf{B}|, \tag{1}$$

where ε is the smallness parameter, generally chosen to be $\approx 10^{-5}$–10^{-4} for computations in the penumbral region. Next, treating the magnetic field at step $n + 1/2$ as a uniform field, we compute the exact helical particle trajectory and carry the particle forward by Δt to position $n + 1$. The process then repeats.

More precisely, at step n we have the particle position and velocity vectors, $\mathbf{x}_n$ and $\mathbf{V}_n$, and we know the current time step size Δt_n. We also have retained the previous field point $\mathbf{x}_{n-1/2}$ as well as the value of the model magnetic field at that point $\mathbf{B}_{n-1/2}$. The particle is carried from step n to $n + 1$ as follows: (1) Compute the new field position,

$$\mathbf{x}_{n+1/2} = \mathbf{x}_n + \mathbf{V}_n \Delta t_n / 2. \tag{2}$$

(2) Determine the magnetic field at the new field point, $\mathbf{B}_{n+1/2}$, using the Tsyganenko and appropriate internal field models. (3) Determine the new time step size from

$$\frac{|\mathbf{B}_{n+1/2} - \mathbf{B}_{n-1/2}|}{|\mathbf{x}_{n+1/2} - \mathbf{x}_{n-1/2}|} V \Delta t_{n+1} = \varepsilon |\mathbf{B}_{n+1/2}|. \tag{3}$$

(4) Carry the particle forward a time Δt_{n+1} to a new position and velocity, $\mathbf{x}_{n+1}$ and $\mathbf{V}_{n+1}$, along an exact helical trajectory computed using the field $\mathbf{B}_{n+1/2}$ (but using $\mathbf{x}_n$ and $\mathbf{V}_n$ as initial conditions).

Finally, we need to explain how to get the process started. Initial position and velocity, $\mathbf{x}_0$ and $\mathbf{V}_0$, are of course given. The initial time step is

$$\Delta t_0 = (L/V)\varepsilon, \tag{4}$$

where

$$\frac{1}{L} = \frac{3}{r} \frac{(1 + 6\cos^2\theta + 9\cos^4\theta + \cos^2\theta \sin^2\theta)^{1/2}}{(1 + 3\cos^2\theta)}, \tag{5}$$

and where r is the initial radial position of the particle and θ is the initial colatitude. This formula is motivated by a dipole approximation to the initial field gradients. With Δt_0 known, the first field position and vector, $\mathbf{x}_{1/2}$ and $\mathbf{B}_{1/2}$, can be computed as described above. Then, equation (3) is used (with $n = 0$) to determine the new time step size Δt_1, except that the initial position $\mathbf{x}_0$ and magnetic field at the initial position $\mathbf{B}_0$ are used in place of $\mathbf{x}_{1/2}$ and $\mathbf{B}_{1/2}$. From this point on the procedure repeats normally.

Simulated Trajectories

Several versions of the Tsyganenko model for the external magnetic field are available. The one employed here is from *Tsyganenko* [1987]. The magnetic field measurements used in developing this model span the range from 4 to 70 R_E and comprise a total of 36,682 vector averages, including the 12,616 points on which the *Mead and Fairfield* [1975] model was based. These data were divided into six groups corresponding to different ranges of the *Kp* index. The external magnetospheric field is constructed from three fields having different sources. The first comes from the ring current, the second from the magnetotail current system (including the plasma sheet current and return current), and the third from magnetopause currents and an averaged contribution from the large-scale system of field-aligned currents. The internal geomagnetic field used in this paper is obtained by interpolating the DGRF between epochs 1985 and 1990. Trajectory calculations are performed in the Geocentric Solar Magnetospheric (GSM) coordinates with the x axis (X_{GSM}) pointing from the Earth to the Sun.

Since the Tsyganenko model does not include an explicit model of the magnetopause we added this separately, using in fact two different models for different ranges of *Kp* index: $Kp \leq 2+$ and $Kp \geq 3-$. These magnetopause models are composed of three adjacent parts with X_{GSM} as the axis of symmetry. The magnetopause in the region of positive X_{GSM} is taken to be the surface of a parabola rotated around the Earth-Sun line. The parabola was visually fitted to the noon-midnight field of the combined Tsyganenko/DGRF model for the case of zero tilt angle of the geomagnetic dipole. The second part of the magnetopause model, from $X_{GSM} = 0$ to $X_{GSM} = -20\ R_E$, is the surface of a cone that was also visually fitted to the noon-midnight field lines. The final part of the model is a cylinder located beyond $X_{GSM} = -20\ R_E$ with a diameter equal to that of the adjacent cone.

Season and time of day affect our trajectory simulations through the changing location of the observation point relative to the subsolar point and through the changing tilt angle of the geomagnetic dipole [*Russell*, 1971]. We also account for variations in geomagnetic activity as characterized by the *Kp* index. Other aspects of space weather will influence the actual trajectories but are not specifically included in the model. Our code is arranged to calculate Tsyganenko model fields, given an actual *Kp* index, for any time from 1901 through 2099. (Of course, one does not really expect the extrapolation of the DGRF to remain valid over this interval.) A particle is traced backwards in time until it (1) reenters the atmosphere (forbidden trajectory), (2) crosses the model magnetopause or reaches a distance of 30 R_E tailward (allowed trajectory), or

(3) travels a total pathlength of 90 R_E (undetermined trajectory) [*Lin et al.*, 1993].

Figure 1 shows examples of trajectories in each category, calculated vertically backward from Prince Albert (53.22 latitude and 254.07 longitude) at 1200 UT (about 0500 MLT) on August 26, 1987. Forbidden trajectories are shown in the top four panels. In this category both ends of the trajectory lie inside the atmosphere, which for the endpoint of the trajectory is defined as reaching a distance of 100 km above the surface of the Earth. Figures 1a and 1b depict the simplest type of forbidden trajectory, for which the observed electrons come from a localized conjugate area in the opposite hemisphere. Figures 1c and 1d illustrate another form of forbidden trajectory. Here a 120-MV splash albedo electron reenters the atmosphere near the point of origin after mirroring in the magnetosphere. Electrons near this energy observed at the balloon are also return albedo but from a less well defined point of origin.

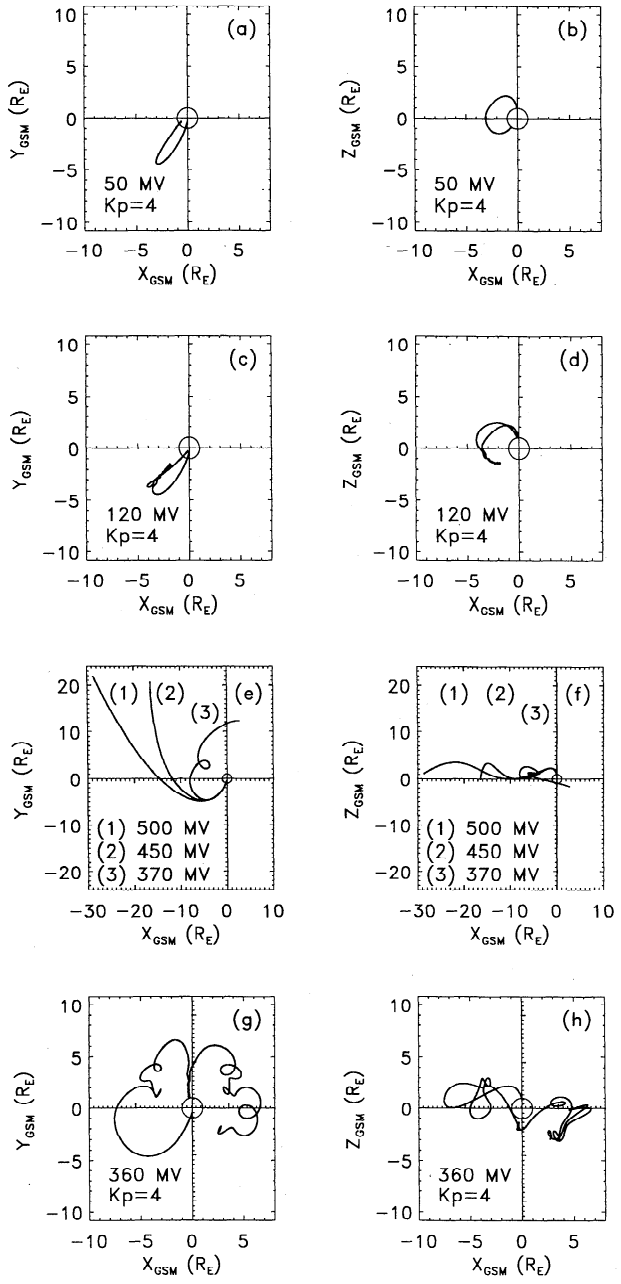

Figure 1. Illustration of trajectory calculations for the indicated rigidities. Trajectories, shown in orthogonal projections, are for electrons vertically incident over Prince Albert at 1200 UT on August 26, 1987, for $Kp = 4$. (a)–(d) Two different kinds of forbidden trajectory. (e) and (f) Illustrations of allowed trajectories. (g) and (h) An undetermined trajectory traced to total pathlength of 90 R_E.

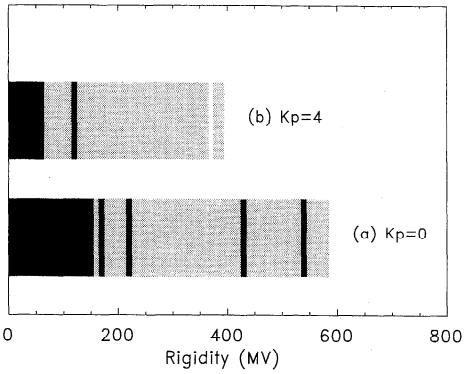

Figure 2. Summary of vertical cutoff rigidity calculation for Prince Albert at 1200 UT on August 26, 1987. Forbidden (dark), allowed (white), and undetermined (patterned) trajectories are shown (a) for geomagnetic quiet condition ($Kp = 0$) and (b) for geomagnetic active conditions ($Kp = 4$).

Figures 1e and 1f show allowed trajectories. They have one end inside the atmosphere, while the other end clearly meets the magnetopause or magnetotail. It is obvious that these trajectories also represent the entry of cosmic particles with rigidities higher than the geomagnetic cutoff through the magnetosphere down to the balloon altitude.

An undetermined trajectory is shown in Figures 1g and 1h. After tracing this 360-MV electron for a pathlength of 90 R_E we find that the particle neither meets the magnetopause nor reenters the atmosphere. Particles such as this follow very complicated trajectories and may drift around the Earth several times. One difficulty in tracing particles for greater distances in a model magnetic field is limited computer time, but a more fundamental problem is that the integration becomes unstable.

Figure 2 illustrates the calculated penumbral structure for particles vertically incident over Prince Albert under active ($Kp = 4$, top) and quiet ($Kp = 0$, bottom) geomagnetic conditions. Increased geomagnetic activity converts some undetermined trajectories to clearly allowed ones and some forbidden trajectories to undetermined ones. In both cases, however, the undetermined trajectories span a very large range. Conclusions about vertical cutoff rigidities will obviously depend critically upon whether these undetermined trajectories are forbidden (the conventional assumption) or allowed. Our balloon observations of cosmic and albedo electrons provide new insights into this important issue.

Electron Observations

Low energy electron (LEE) is a balloon-borne instrument designed to measure electron energy spectra from 15 MeV to 15 GeV with the primary objective of studying long-term changes of the cosmic electron spectrum under the influence of solar modulation [*Hovestadt et al.*, 1970; *Fulks and Meyer*, 1974;

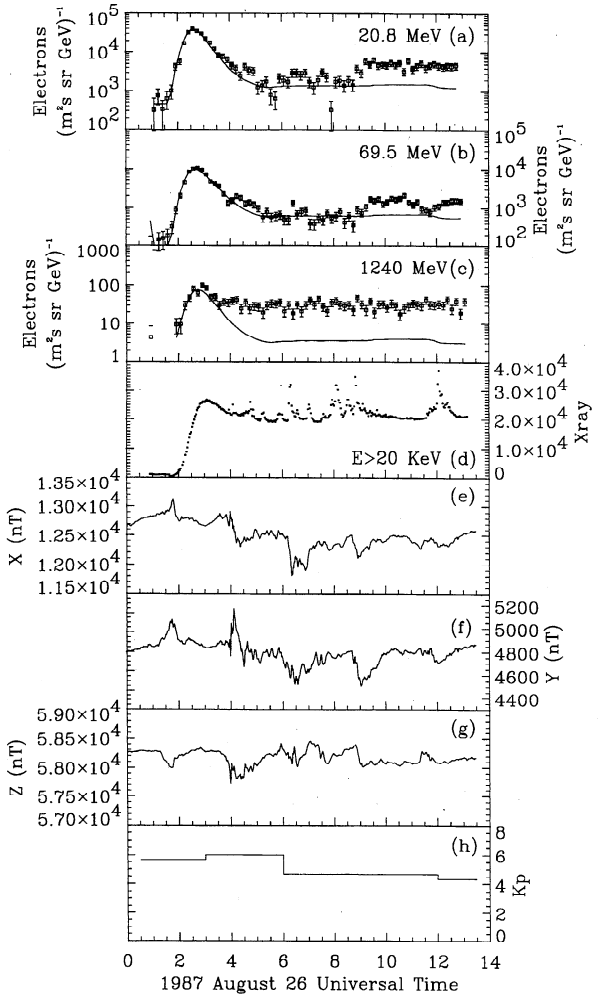

Figure 3. (a)–(c) Measured electron fluxes at 20.8, 69.5, and 1240 MeV (nominal energy). Solid lines show estimated atmospheric secondary electron flux. (d) X rays measured by the balloon-borne detector; (e)–(g) magnetometer data from Meanook; (h) the observed *Kp* index.

Tuska, 1990]. LEE has been flown successfully many times since 1968. As part of this program, it was flown from Prince Albert, Manitoba, on August 26, 1987, significantly south of the usual launch site (Lynn Lake, Manitoba). During this flight the geomagnetic field was very disturbed, and an intense auroral display (from about 0400 to 1000 UT on August 26) was observed from the ground. X ray bursts were recorded simultaneously by the monitoring counters on the payload.

Figure 3 summarizes the observations made on that flight. The top three panels show electron fluxes in three of the energy ranges (nominally 20.8, 69.5, and 1240 MeV) used in our standard analysis. Corrections for atmospheric secondary electrons have not been applied, so the ascent of the balloon through the Pfotzer maximum is apparent in each channel. For reference we show estimates of the atmospheric secondary electrons derived by fitting the calculations of *Daniel and Stephens* [1974] to the Pfotzer maximum. The different time behavior of the electron flux at different energies reveals both the source of the observed electrons and their relation to the geomagnetic cutoff. The highest energy plotted, 1240 MeV, is comfortably above the expected geomagnetic cutoff in Prince Albert. Electrons in the 1240-MeV channel (c) are a combination of galactic electrons and atmospheric secondaries. Neither of these is affected by the disturbed geomagnetic field.

The constancy of the flux of 1240-MeV electrons also provides confirmation that the instrument was operating properly throughout the time interval under consideration. The instrument operates by detecting each electron individually with a trigger system consisting of plastic scintillators and a gas Cherenkov counter all viewed by photomultipliers. The energy of each particle is determined by other photomultipliers viewing a cesium iodide crystal and a lead glass calorimeter. Failures of any kind in this system would almost certainly show up as fluctuations in the apparent flux of 1240-MeV electrons.

Prior to about 0900 UT the geomagnetic cutoff was apparently quite low. The observed electron fluxes at 20.8 MeV (Figure 3a) and 69.5 MeV (Figure 3b) consisted of atmospheric background, which at these energies is higher than and completely obscures the galactic flux. After 0900 UT the 20.8-MeV channel rose to a level characteristic of the return albedo flux, which at this energy is much higher than the atmospheric background. We interpret this to mean that the geomagnetic cutoff rose above 20 MV at approximately 0900 UT and remained higher than 20 MV for the rest of the flight.

Around 0900 UT the 69.5 MeV flux also made a transition from the atmospheric secondary level to the much higher return albedo level. However, between 1100 and 1200 UT the flux dipped (reduced by approximately 50% at 1140 UT) to a value intermediate between the atmospheric secondary and albedo levels. This observation suggests that 70 MV may be associated with some identifiable feature of the penumbral region at this particular point in space and time. Hence we focus the remainder of our discussion on an interpretation of what was happening during this episode.

As seen from the *Kp* index (Figure 3h), August 26 was very disturbed magnetically. In fact, it was the most active day of the month. The three-hourly *Kp* indices between 0000 and 2100 UT were all $\geq 4-$, and were $\geq 5-$ from 0000 to 1200 UT. Figures 3e–3g show magnetometer data recorded in Meanook, Alberta (54.62° geographic latitude, and 246.67° geographic longitude), the nearest magnetometer station to Prince Albert. The ground data exhibit strong geomagnetic disturbances from 0120 to 0200 UT, 0400 to 0500 UT, 0600 to 0720 UT, and 0840 to 0930 UT. A smaller geomagnetic disturbance occurred from 1050 to 1300 UT. X ray bursts (Figure 4d) were observed when geomagnetic activity was intense, at about 0440, 0610, 0700, 0800, 0900, and 1200 UT. These X ray bursts were detected by a plastic scintillator on the balloon experiment with a threshold of approximately 20 keV and an area of approximately 800 cm^2.

Discussion

Our calculations (Figure 2) show that enhanced activity should reduce the cutoff, but the predicted reduction is not sufficient to explain the observations. Specifically, under quiet geomagnetic conditions (*Kp* = 0) the effective vertical cutoff as defined by *Shea and Smart* [1965] for Prince Albert at 1200 UT is calculated to be 585 MV [*Lin et al.*, 1993], using the standard assumption that undetermined trajectories are forbidden. This value is consistent with the effective cutoff ~700 MV derived from isorigidity contours computed by *Smart et al.* [1969b] using the *Williams and Mead* [1965] magnetosphere model. With the disturbance level actually observed after 1200 UT (*Kp* = 4), the

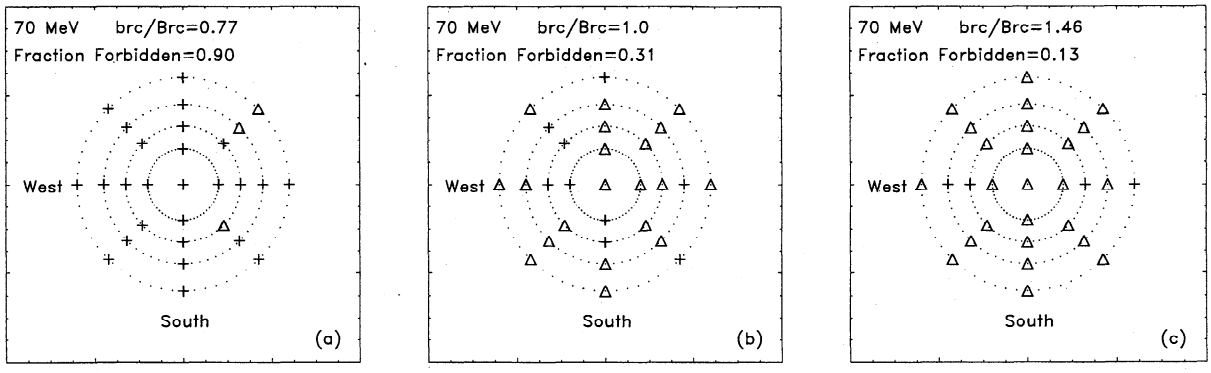

Figure 4. "Sky map" of 70-MeV electron trajectories for Prince Albert at 1200 UT on August 26, 1987, and geomagnetic active condition ($Kp = 4$). The three panels display computations for (a) suppressed, (b) nominal, and (c) enhanced values of the ring current parameter b_{rc}. Dotted circles represent zenith angles of 8°, 13°, 18°, and 24°. Plus signs denote forbidden trajectories, and triangles denote undetermined trajectories.

calculated effective vertical cutoff is reduced significantly to 385 MV, but this is still far above the observed value.

We next considered a more refined model that includes the finite angular response of the instrument and that in addition can simulate short-term magnetospheric variations by modifying the ring current parameter of the Tsyganenko model. Our motivation was twofold. First, we wished to determine whether a comparatively modest alteration of the field model could produce better agreement between predicted and observed cutoffs. Second, we hoped to develop a capability for modeling short-term variations of the electron flux like those observed between 1100 and 1200 UT on August 26, 1987. For most of this time interval, the flux was at values intermediate between the albedo and cosmic/secondary levels. Including oblique directions of incidence and a finite angular response allows for such intermediate levels, since some directions viewed by the detector can be allowed while others are forbidden. Including short-term magnetospheric variations (note Meanook data in Figure 3) is necessary if we are to explain electron flux variations of geomagnetic origin occurring on timescales shorter than the 3-hour timescale of the Kp index.

To model the short-term activity, we vary the ring current parameter, (b_{rc}) within a physically acceptable range about its nominal [*Tsyganenko*, 1987] value (B_{rc}). This parameter is one of 32 employed in the Tsyganenko model and is meant to represent the magnitude of the field depression produced at the center of the ring current. We caution against a literal interpretation of this procedure, however. The parameter b_{rc} is chosen simply because it provides a convenient method for fine tuning the Tsyganenko model. In actuality, the ring current is but one of many factors that determine the instantaneous state of the magnetosphere.

Figure 4 illustrates our calculations for three choices of ring current parameter. The nominal Tsyganenko value is used in Figure 4b, while Figures 4a and 4c respectively depict a 23% depression and 46% enhancement of the ring current. Each panel shows the trajectory type, forbidden (pluses) or undetermined (triangles), for 29 different angles of incidence spread over the 25° opening half-angle of the LEE detector. An overall figure of merit is given by the fraction of forbidden trajectories shown at top of each panel. The fraction of forbidden trajectories decreases with increasing ring current, but there are still no clearly allowed trajectories at this energy.

Albedo "electrons" are actually an almost equal mixture of positrons and negative electrons. Because of their opposite charge sign, the positrons take completely different trajectories from those of electrons. However, the response of the positrons to geomagnetic activity is very similar to that of the electrons. Figure 5 summarizes our calculations and also illustrates the calculation for positrons and electrons separately.

The lower and upper scales give the assumed ring current both in absolute units and relative to the nominal value (for $Kp = 4$) of −43.49 nT in the Tsyganenko model. Trajectories of 20-MeV positrons and electrons are all forbidden for the range of b_{rc} considered. Trajectories of 1240-MeV electrons and positrons are all allowed for this range. At 70 MeV, both electrons and positrons show a significant decrease in the fraction of truly forbidden trajectories with strengthened ring current, but these trajectories have been converted from truly forbidden to computationally "undetermined" trajectories which are normally assumed to be forbidden as well.

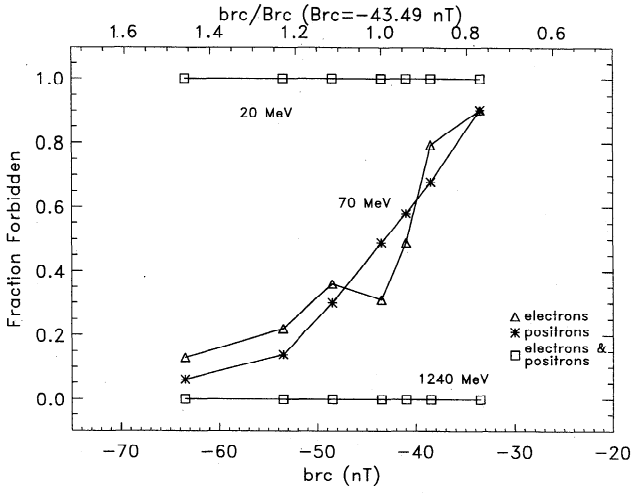

Figure 5. Fraction of forbidden trajectories for positrons and electrons as a function of ring current strength, b_{rc}, for geomagnetic active conditions. Asterisks are for 70-MeV positrons, and triangles are for 70-MeV electrons. Trajectories of 20-MeV positrons and electrons (squares) are all forbidden, and trajectories of 1240-MeV positrons and electrons are all allowed. Upper scale shows ring current strength, (b_{rc}) relative to the nominal Tsyganenko value (B_{rc}).

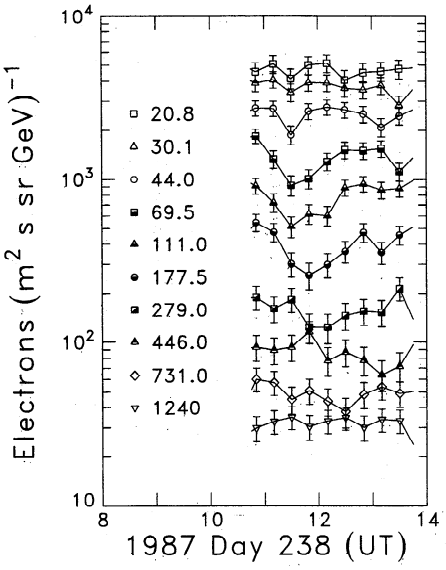

Figure 6. Expanded view, in time and energy, of the time interval discussed in detail in the text. Energies are the nominal mean energies of the analysis channels.

To explain the electron observations, we are therefore led to abandon the conventional assumption that computationally undetermined trajectories are in reality forbidden. We conclude that at least some of the computationally undetermined trajectories are systematically converting, on a short timescale, from physically forbidden to physically allowed. Under this assumption, the Tsyganenko model predicts that 70-MV electrons at 1200 UT with $Kp = 4$ are near the lower boundary of the penumbral region. Short-term magnetospheric variations coupled with finite angular and energy response of the detector can then in principle explain the variation of electron flux observed from 1100 to 1200 UT on August 26, 1987.

A truly detailed look at the phenomenon is precluded by counting statistics, but some insight may be gained from the expanded view shown in Figure 6. Here we show data returned by the instrument in 10 energy channels between approximately 15 and 1500 MeV chosen to have similar statistical accuracy. While the 44-MeV channel may show a brief fluctuation, transitions away from the return albedo flux and back are clearly apparent in the channels from 69.5 MeV through 177.5 MeV. The transition is arguably present in the 279-MeV channel. Unfortunately, the 449-MeV channel (at this phase of the solar modulation cycle) has little contrast between the cosmic and return albedo fluxes. The lack of fluctuation at this energy therefore gives no information. At 731 MeV and above (where the return albedo would be markedly lower than the cosmic flux) there is no indication of variability, so this is an upper limit on where the cutoff lies. What this suggests is that some magnetospheric process operative during this episode had the effect of converting some but not all physically forbidden trajectories into allowed ones throughout most (70–279 MV) if not all of the computationally "undetermined" region. Our ability to determine the actual fraction of trajectories converted and the dependence of this fraction on time and energy is limited, and we do not quote specific estimates.

The computational indeterminacy of this region thus appears to have a counterpart indeterminacy in physical reality, in the sense that trajectories easily change character under disturbed conditions in a manner which does not emerge from the Tsyganenko model or from the simple manipulations of the model that we have investigated. Nevertheless, in our view, our interpretation supports the basic validity of the Tsyganenko model, since the model predicts the existence and extent of a band of computationally undetermined trajectories that appears to have some physical reality, and some underlying organizing parameter. What this parameter might be is beyond the scope of our investigation, but as an example of what one might investigate, we note that we have not considered in any detail the validity of our assumption that electric fields are negligible. Systematic changes in even a small electric field that ordinarily appears second order might well provide a small perturbation to convert these convoluted trajectories from forbidden to allowed.

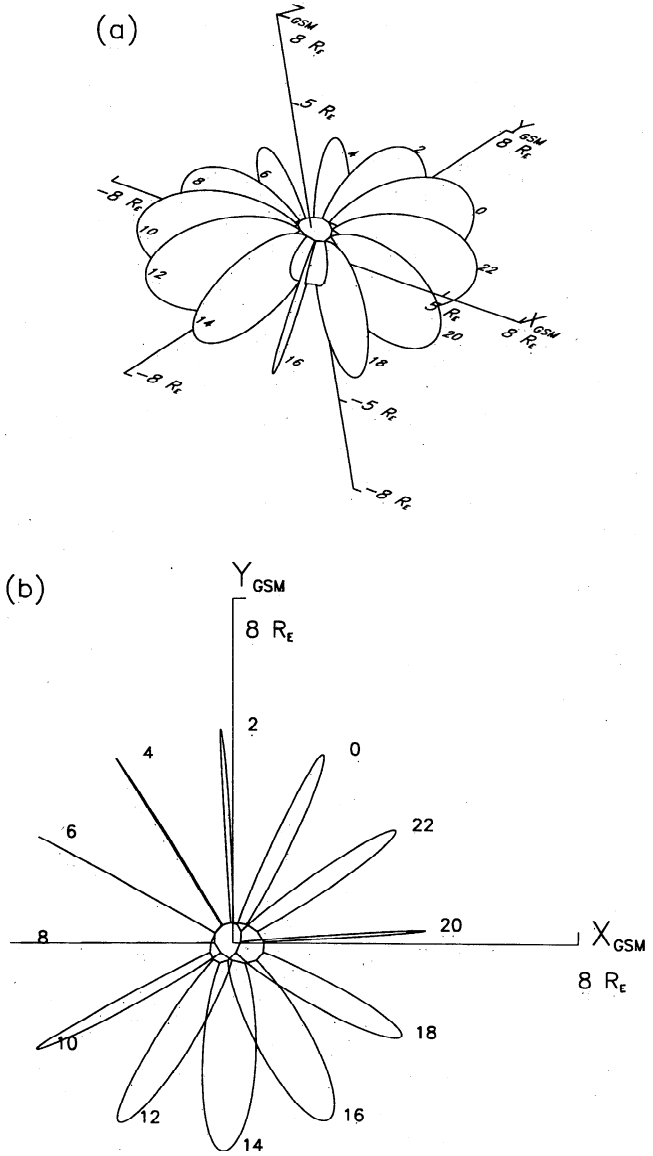

Figure 7. (a) Geomagnetic field lines at different times on August 26, 1987, at Prince Albert, Canada. The number next to each field line is the universal time. (b) Projections of the field lines on the XY plane. The rightmost central ellipse is the intersection of the field lines with the Earth in the northern hemisphere and the leftmost central ellipse is the intersection of the field lines with the Earth in the southern hemisphere.

If we accept the validity of the Tsyganenko model at this time we are lead to a further conclusion concerning the X ray burst observed on the flight, including the large X ray burst centered at 1200 UT that seems to terminate the entire fluctuating cutoff phase of our observations. Figure 7a presents a three-dimensional view of the model geomagnetic field lines for different times at Prince Albert, Canada, while Figure 7b shows the projection of these field lines on the XY plane. The varying Kp index and geomagnetic tilt angles as functions of time were taken into account. The number next to each field line is the corresponding universal time. The geomagnetic field line of 0800 UT (about local midnight) is on the XZ plane and extends in the radial direction to a maximum of about 5.2 R_E. The field line of 2000 UT (about local noon) is compressed a little and has a maximum radial extent of about 4.5 R_E. Successive X ray bursts were observed on the ground and recorded by the balloon-borne monitor counters between 0400 and 1300 UT roughly correlated with geomagnetic disturbance (Figure 3). However, at no time does the model predict a significant change in the L value for Prince Albert on that day. Our results imply that the precipitating electrons responsible for these bursts originated in the radiation belts, which is in contrast to earlier observations of precipitating electrons near open field lines ($L \approx 10$) [*Matthews et al.*, 1988]. The implication is clearly that the electrons producing these X rays came from deep within the magnetosphere. Specifically, we conclude that they were accelerated at (or precipitated from) $L = 5$. It is possible that a significant rearrangement of the magnetosphere (reconnection event?) at the time of the final large burst was related to the seemingly permanent return of undetermined trajectories to their normal (forbidden) state from their disturbed (allowed) state.

Acknowledgments. We thank M. A. Shea, D. F. Smart, and E. Tuska for useful discussion. It is a pleasure to thank J. L'Heureux in particular for many stimulating discussions. We thank D. J. McEwen of the University of Saskatchewan and L. Morris of National Geophysical Data Center for assistance procuring Meanook magnetometer data. This work was supported by NSF grants OPP-9219761, ATM-9115492, and ATM-9314683.

The Editor thanks J. P. Wefel and E. O. Flückiger for their assistance in evaluating this paper.

References

Berger, M. J., and S. M. Seltzer, Bremsstrahlung in the atmosphere, *J. Atmos. Terr. Phys.*, *34*, 85–108, 1972.

Bieber, J. W., P. Evenson, and Z. M. Lin, Cosmic ray trajectories in the Tsyganenko magnetosphere, *Antarctic J.*, *27*(5), 318–319, 1992.

Cooke, D. J., J. E. Humble, M. A. Shea, D. F. Smart, N. Lund, I. L. Rasmussen, B. Byrnak, P. Goret, and N. Petrou, On cosmic-ray cutoff terminology, *Nuovo Cimento. Soc. Ital. Fis. C*, *14*, 213–234, 1991.

Daniel, R. R., and S. A. Stephens, Cosmic ray produced electrons and gamma rays in the atmosphere, *Rev. Geophys.*, *12*, 233–258, 1974.

Flindt, H. R., Local time dependence of geomagnetic cutoffs for solar protons $0.52 \leq E_p \leq 4$ MeV, *J. Geophys. Res.*, *75*, 39–49, 1970.

Flückiger, E. O., E. Kobel, D. F. Smart, and M. A. Shea, A new concept for the simulation and visualization of cosmic ray particle transport in the Earth's magnetosphere, *Proc. Int. Conf. Cosmic Ray 22nd*, *3*, 648–651, 1991.

Fulks, G., and P. Meyer, Cosmic ray electrons in the atmosphere, *J. Geophys.*, *40*, 751–759, 1974.

Gall, R., J. Jimenez, and L. Camacho, Arrival of low-energy cosmic ray via the magnetospheric tail, *J. Geophys. Res.*, *73*, 1593–1605, 1968.

Gall, R., A. Orozco, C. Marin, A. Hurtado, and G. Vidargas, Tables of approach directions and points of entry of cosmic rays for higher latitude cosmic rays stations, Univ. Nacional Autonoma de Mexico, Inst. de Geofis., Mexico City, 1982.

Guzik, T., Y. Sang, J. P. Wefel, and J. F. Cooper, Limits on charge states of high energy solar flare ions measured in 1982 by the Phoenix-1 experiment, *Proc. Int. Conf. Cosmic Ray 22nd*, 656, 1991.

Hovestadt, D., and P. Meyer, The geomagnetic cutoff at Ft. Churchill and the primary cosmic electron spectrum from 10 MeV to 12 BeV in 1968, *Acta Phys. Hung. Suppl. 2*, *29*, 525–531, 1970.

Hovestadt, D., P. Meyer, and P. Schmidt, A detector system for cosmic ray electrons, *Nucl. Instrum. Methods*, *85*, 93–100, 1970.

Imhof, W. L., J. B. Reagan, and E. E. Gaines, Solar particle cutoffs as observed at low altitudes, *J. Geophys. Res.*, *76*, 4276–4290, 1971.

Israel, M. H., Cosmic ray electrons between 12 MeV and 1 GeV in 1961, *J. Geophys. Res.*, *74*, 4701–4713, 1969.

Israel, M. H., and R. E. Vogt, Flux of cosmic-ray electrons between 17 and 63 MeV, *Phys. Rev. Lett.*, *20*, 1053–1056, 1968.

Jokipii, J. R., J. L'Heureux, and P. Meyer, Diurnal intensity variation of low-energy electrons observed near the polar cap, *J. Geophys. Res.*, *72*, 4375–4382, 1967.

Langel, R. A., International Geomagnetic Reference Field, 1991 Revision, *IAGA News*, no. 30, 1991.

Lin, Z. M., J. W. Bieber, and P. Evenson, Cosmic ray trajectories over Prince Albert: Albedo electron measurements and model calculations, *Proc. Int. Conf. Cosmic Ray 23rd*, *3*, 777–780, 1993.

Matthews, D. L., T. J. Rosenberg, J. R. Benbrook, and E. A. Bering III, Dayside energetic electron precipitation over the South Pole, *J. Geophys. Res.*, *93*, 12941–12945, 1988.

McCracken, K. G., U. R. Rao, and M. A. Shea, The trajectories of cosmic rays in a high simulation of geomagnetic field, *Rep. 77*, Mass. Inst. of Technol., Cambridge, Aug. 1962.

Mead, G. D., and D. H. Fairfield, A quantitative magnetospheric model derived from spacecraft magnetometer data, *J. Geophys. Res.*, *80*, 523–534, 1975.

Pfotzer, G., Dreifachkoinzidenzen der Ultrastrahlung aus vertikaler Richtung in der Stratosphare, I, Messmethode und Ergebnisse, *Z. Phys.*, *102*, 23–40, 1936a.

Pfotzer, G., Dreifachkoinzidenzen der Ultrastrahlung aus vertikaler Richtung in der Stratosphare, II, Analyse der gemessenen Kurve, *Z. Phys.*, *102*, 41–58, 1936b.

Russell, C. T., Geophysical coordinate transformations, *Cosmic Electrodyn.*, *2*, 184–196, 1971.

Sauer, H. H., A new method of computing cosmic-ray cutoff rigidity for several geomagnetic field models, *J. Geophys. Res.*, *68*, 957–971, 1963.

Shea, M. A., and D. F. Smart, Worldwide trajectory-derived cutoff rigidities and their application to experimental measurements, *J. Geophys. Res.*, *72*, 2021–2027, 1967.

Shea, M. A., and D. F. Smart, Variation of the calculated cosmic-ray equator over a 20-year interval, *Proc. Cosmic Ray Conf. Int. 14th*, *4*, 1294–1297, 1975.

Shea, M. A., and D. F. Smart, The influence of the changing geomagnetic field on cosmic ray measurements, *J. Geomagn. Geoelectr.*, *42*, 1107–1121, 1990.

Shea, M. A., D. F. Smart, and K. G. McCracken, A study of vertical cutoff rigidities using sixth degree simulations of the geomagnetic field, *J. Geophys. Res.*, *70*, 4117, 1965.

Smart, D. F., M. A. Shea, and R. Gall, The daily variation of trajectory-derived high-latitude cutoff rigidities in a model magnetosphere, *J. Geophys. Res.*, *74*, 4731–4738, 1969a.

Smart, D. F., M. A. Shea, and R. Gall, Iso-rigidity contours in the polar region interpolated from trajectory-derived vertical cutoff rigidities, *Proc. Conf. Int. Cosmic Ray 11th*, *29*, 601–604, 1969b.

Tsyganenko, N. A., Global quantitative models of the geomagnetic field in the cislunar magnetosphere for different disturbance levels, *Planet. Space Sci.*, *35*, 1347–1358, 1987.

Tuska, E. B., Charge-sign dependent solar modulation of 1–10 GV cosmic rays, Ph.D. thesis, Univ. of Del., Newark, 1990.

Verma, S. D., Measurement of the charged splash and reentrant albedo of the cosmic radiation, *J. Geophys. Res.*, *72*, 915–925, 1967.

Williams, D. J., and G. D. Mead, Nightside magnetosphere configuration as obtained from trapped electrons at 1100 kilometers, *J. Geophys. Res.*, *70*, 3017–3029, 1965.

J. W. Bieber, P. Evenson, and Z. Lin, Bartol Research Institute, University of Delaware, Newark, DE 19716.

(Received May 18, 1995; revised August 24, 1995;
accepted August 29, 1995.)